Voloshina and Dedkov *NPG Asia Materials* (2026)18:6
https://doi.org/10.1038/s41427-026-00633-y

NPG Asia Materials

REVIEW ARTICLE Open Access

Substrate-induced magnetism in graphene: a minireview

Elena Voloshina[1] and Yuriy Dedkov[2]

Abstract

Recent discoveries of substrate-induced magnetism in graphene layers, along with subsequent advancements in the field, have garnered significant attention due to their potential applications in spintronics and sensing technologies. Moreover, further studies have revealed a remarkable tunability of the electronic and magnetic properties in graphene/substrate systems - not only is graphene's electronic structure influenced by the substrate, but graphene itself can also modify the properties of the underlying material. In this minireview, we highlight several representative examples illustrating the impact of graphene adsorption on ferromagnetic substrates (metals, semiconductors and insulators), where induced magnetism in graphene has been observed. A critical analysis of both experimental and theoretical findings is presented, offering insights and outlining future directions in this rapidly evolving area.

Introduction

The discovery, two decades ago, of the remarkable transport properties of graphene (gr)[1–3] sparked extensive experimental and theoretical investigations into the electronic, magnetic, and optical properties of various two-dimensional (2D) materials. Among them, graphene remains at the forefront of research due to its unique gapless electronic structure, characterized by a linear $E(k)$ dispersion near the Fermi level. This structure can be readily tuned owing to the low density of electronic states, enabling phenomena such as band-gap opening, wide-range modulation of the doping level, and the induction of spin polarization for the charge carriers[4–6]. One particularly intriguing aspect is the potential for establishing long-range ferromagnetic - or more generally, magnetic - order in a single graphene layer.

A free-standing graphene layer, composed of light carbon atoms (low atomic number Z), lacks intrinsic magnetic moments, and the electron exchange interaction does not fulfill the Stoner criterion for the emergence of long-range ferromagnetic order. Nevertheless, experimental studies have demonstrated the feasibility of long-range spin transport in both single- and bilayer graphene when using ferromagnetic (FM) materials, such as cobalt or permalloy films, as spin injection contacts. Spin diffusion lengths reaching several tens of micrometers at room temperature have been reported[7,8]. Furthermore, theoretical predictions suggest that multilayer graphene can function as an effective spin filter in FM/gr/FM junctions, emphasizing the role of the induced exchange interaction at the gr/FM interface[9,10]. This effect was recently confirmed experimentally in Ni/gr/Ni(111) nanojunctions[11].

Following the discovery of graphene's intriguing transport properties, various strategies have been proposed to induce long-range (ferro)magnetic order in an effort to realize an ideal two-dimensional (2D) (ferro)magnet. These approaches include defects' engineering[12–14], adsorption of different atomic or molecular species[15,16], and the exploitation of quantum confinement effects in graphene dots or nanoribbons[17,18], among others[19]. However, experimental studies have shown that the most straightforward and effective method for inducing long-range (ferro)magnetic order in graphene is its adsorption onto ferromagnetic or antiferromagnetic substrates (Fig. 1). This leads to induced magnetism in graphene either through electron exchange interactions or/and via proximity effects from the magnetically ordered substrate[20].

Given the broad range of potential applications of (ferro)magnetically ordered graphene layers and the

Correspondence: Elena Voloshina (elena.voloshina@irb.hr) or Yuriy Dedkov (ydedkov@ifs.hr)
[1]Division of Theoretical Physics, Ruđer Bošković Institute, Zagreb, Croatia
[2]Center for Advanced Laser Techniques, Institute of Physics, Zagreb, Croatia

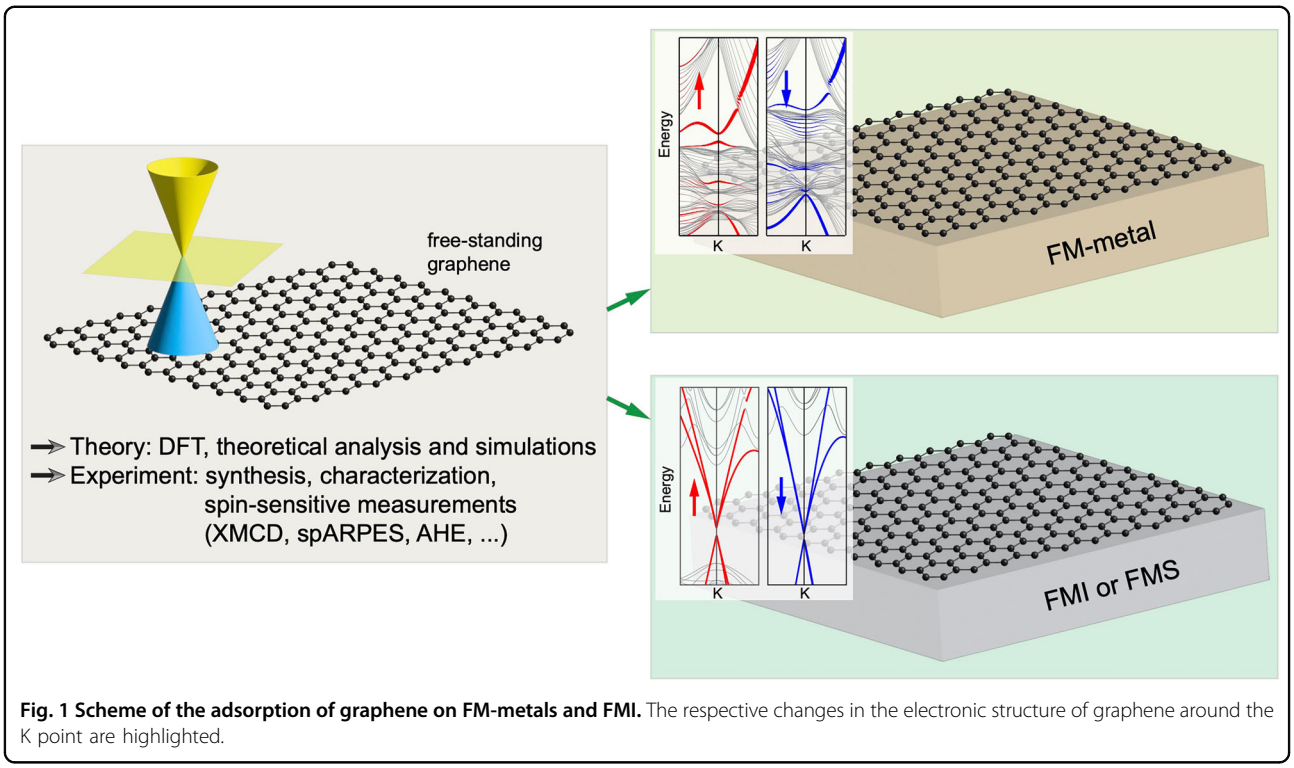

Fig. 1 Scheme of the adsorption of graphene on FM-metals and FMI. The respective changes in the electronic structure of graphene around the K point are highlighted.

fascinating physical phenomena associated with this state in two dimensions, this minireview focuses on specific examples where substrate-induced magnetic order in graphene has been realized. We highlight two common approaches for achieving substrate-induced magnetism in graphene: synthesis or adsorption on metallic ferromagnetic substrates and on ferromagnetic insulators. The underlying mechanisms responsible for magnetic ordering in graphene are discussed in both contexts. Our discussion includes both theoretical and experimental advancements, with particular emphasis on surface science spectroscopic techniques, which provide direct access to spin-resolved electronic structures, and the use of the anomalous Hall effect as an indirect probe of magnetic ordering in 2D layers. Finally, we outline future directions in the study of induced magnetism in two-dimensional materials[21–23], particularly in graphene, and explore how this magnetic state can be engineered for prospective applications in graphene/FM-based systems.

Graphene on FM metals

The first systematic theoretical studies of the gr/FM-Ni(111) system were presented in ref. [24]. As discussed in this and numerous subsequent theoretical and experimental works, the most energetically favorable geometry for graphene on close-packed surfaces such as Ni(111) and Co(0001) is the *top-fcc* configuration. In this arrangement, one carbon atom in the graphene unit cell sits directly above a metal atom at the interface (top position), while the other occupies the *fcc* hollow site of the metallic slab[25–29] (Fig. 2a, b). All theoretical studies predict the presence of an induced magnetic moment in the graphene layer, resulting from strong hybridization between the graphene π orbitals and the spin-polarized FM 3*d* orbitals. For gr/Ni(111), the induced magnetic moments are reported to be approximately −0.01/0.02 μ_B[24] and −0.02/0.04 μ_B[28,29], depending on whether van der Waals (vdW) interactions are included in the GGA-based DFT calculations (two values correspond to carbon atoms in different sublattices). For graphene on Co(0001), the magnetic moments are slightly larger due to the higher intrinsic magnetization of Co atoms compared to Ni[28,30]. Additionally, graphene adsorption on FM surfaces leads to a significant reduction in the magnetic moment of the interface metal atoms, for example, from 0.68 μ_B to 0.518 μ_B for Ni(111) vs. gr/Ni(111), and from 1.731 μ_B to 1.54 μ_B for Co(0001) vs. gr/Co(0001)[24,27,28].

A detailed analysis of the interaction strength between graphene and FM metals, along with the resulting modifications at the interface, reveals significant changes in the electronic structure of both graphene and the substrate. These changes arise primarily from spin-polarized charge transfer at the interface and strong orbital overlap (hybridization) between the electronic states of graphene (specifically the π orbitals) and the spin-polarized 3*d* orbitals of the FM substrate[31]. This hybridization occurs in energy, real-, and *k*-space. The resulting electronic band structure of gr/FM interfaces exhibits a number of

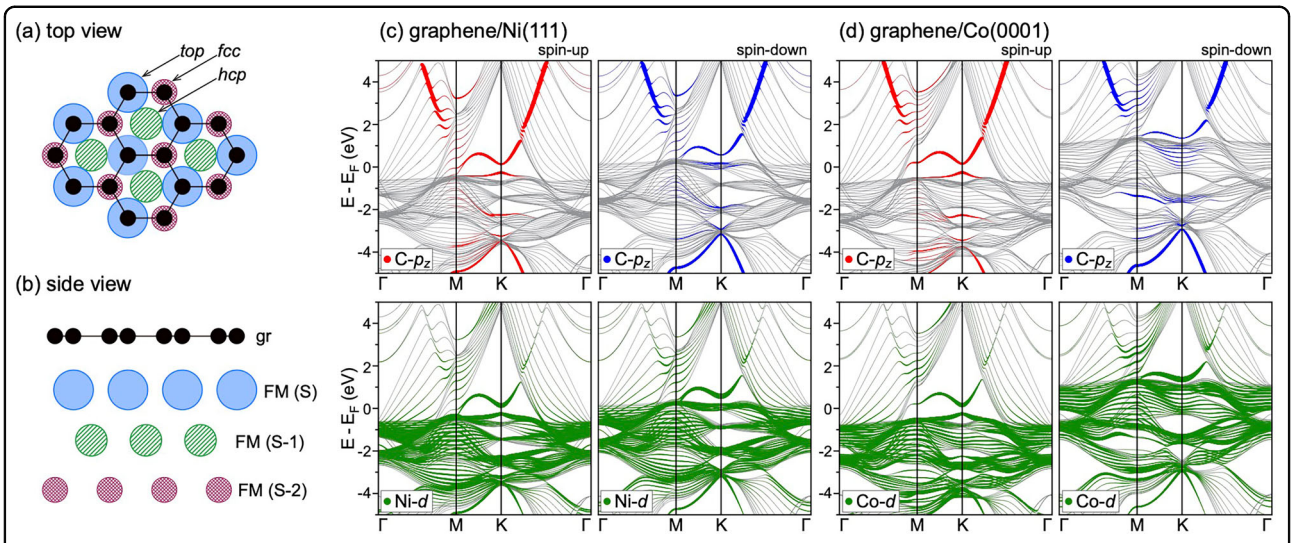

Fig. 2 Electronic structure of graphene on ferromagnetic metals. a Top- and **b** side-view of a ball model for the *top-fcc* arrangement of graphene on close-packed Ni(111) surface. **c**, **d** Calculated spin-resolved band structures for gr/Ni(111) and gr/Co(0001) systems. The radius of the circles is proportional to the partial density of states at the interface between FM and C atoms. Data are reproduced from ref. [28].

so-called interface states, which are predominantly of C p_z and FM 3 d character[24,27,28,32,33] (Fig. 2c, d). As a consequence of the substantial rearrangement of electronic states at the gr/FM interface, the π states of graphene lose their free-standing character and, strictly speaking, can no longer be described as Dirac fermions.

Graphene layers (mono-, bi-, and multilayers) can be directly grown on metallic substrates using the widely accepted method of chemical vapor deposition, which ensures high crystallographic order and purity of the graphene/metal interfaces[34–36]. The first experimental confirmation of an induced magnetic moment in graphene and the observation of a long-range ferromagnetic state in this layer supported on an FM metal substrate were provided by a series of studies employing X-ray magnetic circular dichroism (XMCD) at the C K absorption edge and spin-resolved photoelectron spectroscopy, primarily for the gr/Ni(111) system[37–39] (Fig. 3a, b). These findings were later confirmed for other gr/FM interfaces as well[32,33,40–45]. These experiments consistently demonstrated a parallel alignment of the magnetic moments in graphene and the underlying FM substrate. The exchange splitting of the graphene π band at the Γ point in the gr/Ni(111) system was measured to be approximately 35 meV[38], in very good agreement with DFT-calculated values[24,27,28]. Due to the absence of spin-orbit splitting in the C 1s core level, only the orbital magnetic moment of the C p_z electrons can be directly extracted, yielding a value of $\mu_{orb} = (1.8 \pm 0.6) \times 10^{-3}\ \mu_B$ per carbon atom. Estimates for the corresponding spin magnetic moment lie in the range of 0.05–0.1 μ_B per carbon atom, consistent with theoretical predictions[37–40,42]. Ironically, some studies report relatively giant values for both spin and orbital magnetic moments of carbon atoms in graphene on FM substrates - for example, $\mu_{orb} = 0.062\ \mu_B$ and $\mu_{spin} = 0.412\ \mu_B$ per carbon atom[44,45], or $\mu_{orb} = 0.1\ \mu_B$ per carbon atom[41]. These values are comparable to those found in clean FM materials like Ni and Co[37,46]. In some cases, an unclear distinction between the spin and orbital contributions to the magnetic moment of both carbon atoms and the FM substrate has led to confusion and inconsistencies in the reported results[41,47].

Interestingly, XMCD experiments on the gr/Ni(111) interface revealed that graphene adsorption induces a spin-reorientation of the magnetic moments of interface Ni atoms from the in-plane orientation typical of bulk Ni to an out-of-plane direction. This is accompanied by a reduction inthe total magnetic moment of the Ni atoms - an effect predicted by theory and previously observed in spin-resolved angle-resolved photoemission spectroscopy (spARPES) experiments[37,38,40]. This spin-reorientation is attributed to strong hybridization between graphene π orbitals and Ni 3 d states, which enhances the out-of-plane magnetic anisotropy energy (MAE)[48]. A similar effect—out-of-plane reorientation of magnetic moments at the Co interface and an increase in MAE—was observed in gr/Co systems formed via intercalation of Co beneath graphene on Ir(111)[49,50]. These experiments, conducted using spin-polarized low-energy electron microscopy, enabled detailed tracking of the magnetization behavior in both Co/Ir and gr/Co/Ir interfaces. Theoretical analysis showed that the MAE for the gr/Co interface is approximately twice that of a bare Co film,

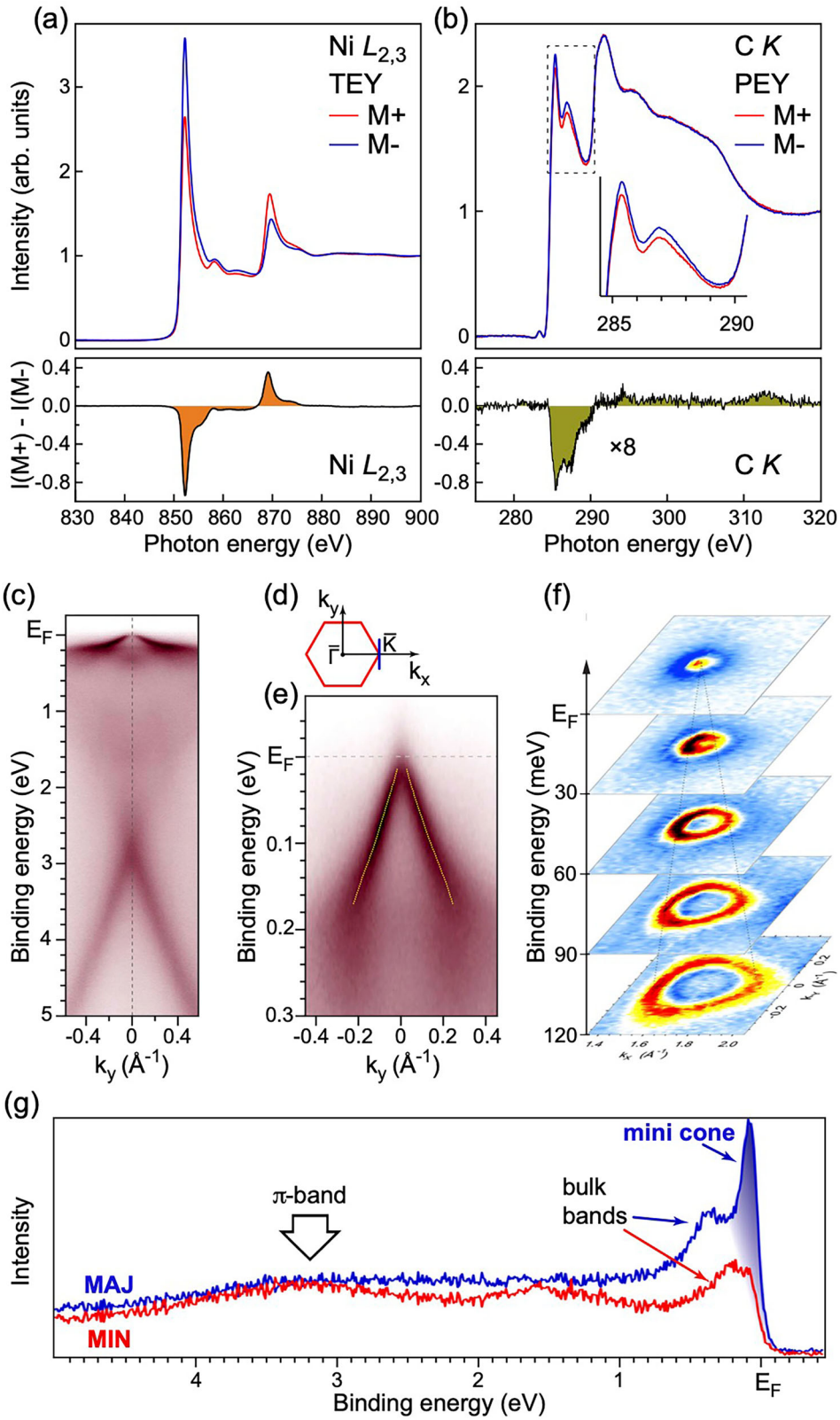

Fig. 3 Spectroscopic studies of graphene on ferromagnetic metals. a, **b** XMCD spectra of gr/Ni(111) measured at the Ni $L_{2,3}$ and C *K* absorption edges demonstrating induced magnetism in graphene. **c**–**e** ARPES intensity maps of gr/Co(0001) collected near K point. **f** The 3D representation $I(k_x, k_y, E_b)$ of the ARPES intensity corresponding to map in (**e**). **g** Spin-resolved ARPES spectrum measured at the K point of gr/Co(0001). Data are reproduced from refs. [32,37].

regardless of the ferromagnetic layer's thickness. Furthermore, graphene adsorption extends the effective out-of-plane anisotropy to an unprecedented thickness of 25 Å. Building on these findings, it was demonstrated that $(Co_n/gr)_m$ superlattices exhibit extremely high perpendicular magnetic anisotropy: for example, 4.6 mJ/m^2 for $(Co_3/gr)_3$, compared to just 0.2 mJ/m^2 for the widely studied $(Co_3/Pt)_3$ system[50]. These results highlight the potential of such graphene-based magnetic heterostructures for future spintronic information processing technologies.

Figure 3c–g shows experimental photoemission intensity maps near the K point, along with a corresponding spARPES spectrum collected at K for the gr/Co(0001) system[32,33]. These data clearly demonstrate the formation of hybrid states at the graphene-Co interface, as predicted by DFT calculations[24,27–29,32,33] (see Fig. 2d). According to these theoretical results, both gr/Ni(111) and gr/Co(0001) interfaces exhibit highly spin-polarized interface states located near the Fermi level at the K point – an observation confirmed by the experimental data (Fig. 3c–g). These interface states have a pronounced two-dimensional character, with a dominant contribution from Ni 3 *d* or Co 3 *d* orbitals – roughly an order of magnitude greater than the contribution from C p_z orbitals. Notably, the linear dispersion typically associated with Dirac fermions is not preserved at the K point. Given this analysis – especially the large Fermi velocity and the lack of linear dispersion – charge carriers in these states cannot, strictly speaking, be described as Dirac fermions without further orbital characterization using tight-binding models. Nevertheless, these results validate earlier theoretical descriptions of the gr/FM interface and offer important insights for understanding spin-polarized phenomena in graphene/FM-metal systems.

Further experimental and theoretical studies of gr/FM systems have focused on identifying strategies to reduce the interaction between graphene and the metallic substrate, while still preserving the induced magnetic ordering in the two-dimensional layer. It has been shown that intercalation of *sp* metals[27,51–53] or other non-metallic species[54–56] can effectively decouple graphene from the FM substrate. However, this typically leads to a suppression of the exchange interaction at the interface. In contrast, intercalation of thin layers of open-shell *d*- or *f*-metals[57], or the use of complex FM substrates such as alloys[30,58,59], can significantly enhance the induced magnetic moment in graphene and alter the spin texture near the Fermi level. For example, intercalating a monolayer (1 ML) of Fe beneath graphene on Ni(111) (gr/1 ML-Fe/Ni(111)) results in a substantial increase in the magnetic moment of the carbon atoms. This is evidenced by a 2.5−3-fold enhancement in the C K-edge XMCD contrast compared to the gr/Ni(111) system[39]. This behavior is attributed to the reduced dimensionality of the intercalated Fe layer, which leads to an increased magnetic moment of Fe atoms and the formation of quantum well states within the intercalated FM layer. Both effects contribute to the enhanced magnetic response of the graphene layer.

The intercalation of open-shell *f*-elements (considered magnetically active) into gr/FM interfaces results in effective decoupling of graphene from the ferromagnetic substrate. As predicted theoretically[57] and later confirmed experimentally[60,61], the use of rare-earth metals such as Eu as intercalants beneath graphene on Co(0001) or Ni(111) leads to the restoration of graphene's band structure near the Fermi level. However, graphene becomes strongly *n*-doped, and a band gap opens directly at the Dirac point. This strong doping results in a downward shift of the π* band and the formation of spin-polarized van Hove singularities near the Fermi level around the M point[57,60,61] (Fig. 4). The spin character of the π^* band is attributed to hybridization between graphene's electronic states and the Eu 5 *d* states, which are magnetically polarized opposite to the Eu 4 *f* states by the presence of the FM Co susbstrate. Interestingly, the $\pi - \pi^*$ gap at the Dirac point in the gr/Eu/FM system becomes spin-dependent. This effect is attributed to the spin-dependent hybridization between graphene's π states and the strongly spin-polarized Eu 4 *f* orbitals.

Another approach for realizing a gr/FM interface was proposed in ref. [58]. In this work, the parent epitaxial gr/Ge interface is modified via Mn intercalation, resulting in the formation of the gr/FM-Mn_5Ge_3/Ge system. The resulting Mn_5Ge_3 alloy is ferromagnetic with a Curie temperature close to room temperature and a high magnetic moment for Mn atoms (approximately 3.5 μ_B), leading to significant exchange splitting in the valence band states. DFT calculations predict a spin-dependent hybridization between the graphene π states and the Mn 3 *d* states. This interaction may lead to a scenario where only spin-up electrons in graphene retain a Dirac-like character near the Fermi level and at the K point. Motivated by this prediction, the gr/FM-Mn_5Ge_3/Ge system was experimentally realized on both (110)- and (111)-oriented Ge substrates[62]. Surprisingly, for both substrate orientations, the resulting gr/FM- Mn_5Ge_3 interfaces exhibit nearly free-standing character for graphene π states with only minimal *n*-doping. The interface shows high crystalline quality and clear ferromagnetic ordering of the thick alloy films. However, further spin-sensitive spectroscopic experiments, such as XMCD or spin-resolved ARPES, are necessary to confirm the intriguing theoretical predictions. If validated, this interface may hold significant promise for applications in electronics or spintronics, especially considering the tunability of the Curie temperature in the FM-Mn_5Ge_3 alloy.

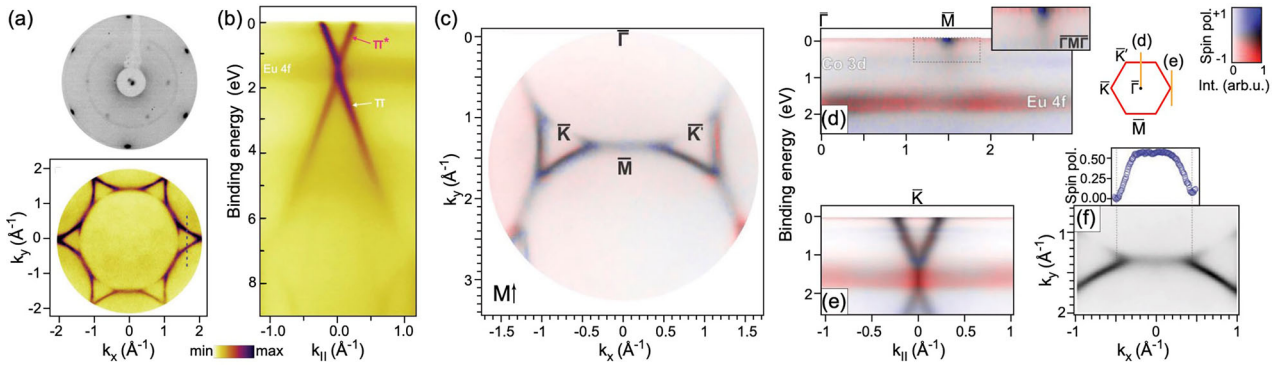

Fig. 4 Modifications of the graphene/FM-metal interfaces. a LEED (top) and Fermi surface (bottom) as well as (**b**) ARPES map collected around K for gr/Eu/Co(0001). **c** Spin-resolved Fermi surface (binding energy 50 meV) of the gr/Eu/Co system. **d** Spin-resolved energy versus momentum map acquired along the Γ—M — Γ direction. Inset shows a zoom of the area indicated by the dashed lines. **e** Spin-resolved energy versus momentum map acquired at the K point. **f** Momentum map of the region near the M point, along with the plot of spin polarization acquired along the flat band (K — M — K′ direction). According to the 2D color code, blue and red intensities correspond to majority and minority electronic states. Data are reproduced from ref. [60].

Graphene on FM semiconductors and insulators

Although the gr/FM-metal systems discussed in the previous sections exhibit many intriguing fundamental properties and serve as an excellent platform for studying various spin-dependent phenomena, the unique electronic properties of graphene are limited in practical use due to the metallic shortcut to the substrate. By integrating a single graphene monolayer with a ferromagnetic insulator (FMI) or ferromagnetic semiconductor (FMS), ferromagnetism can be induced in graphene without compromising its exceptional transport properties. The hybridization between graphene's π orbitals and the spin-polarized orbitals of the adjacent magnetic insulator provides the exchange interaction necessary for long-range ferromagnetic ordering. Importantly, this proximity effect preserves the linear dispersion of graphene bands near the Dirac point. Additionally, unlike ferromagnetic metals, which, in principle, can mediate proximity exchange interactions, magnetic insulators do not divert current away from graphene.

To date, proximity-induced ferromagnetism in graphene has been investigated in numerous gr/FMI and gr/FMS systems, including yttrium and rare-earth iron garnets (YIG and REIG)[43,63–66], Eu-based chalcogenides (EuX, X: O, S)[65,67,68], $Cr_2Ge_2Te_6$ (CGT)[64,69–72], and transition metal phosphorus trichalcogenides (MPX_3 with M = transition metal, X = S, Se)[73,74]. In most experimental studies, the induced magnetism in the graphene layer was probed using the anomalous Hall effect (AHE) method[75]. Since proximity-induced magnetism in 2D layers is often subtle, these investigations require meticulous sample preparation as well as rigorous and critical data analysis[76,77].

When a graphene layer is brought into contact with FMI or FMS and subjected to a strong magnetic field perpendicular to the layer, the transverse resistance R_{xy} consists of two contributions: the ordinary Hall resistance, proportional to the external magnetic field B, and the AHE contribution, proportional to the induced magnetization M in the perpendicular direction. This can be expressed as $R_{xy} = R_H(B) + R_{AHE}(M) = \alpha B + \beta M$[63,75]. Therefore, the resulting $R_{xy}(B)$ shows a linear dependence on the applied magnetic field with superimposed deviations that follow the magnetization behavior of the underlying FMI or FMS. This behavior was clearly demonstrated in early experiments on graphene/YIG systems, where induced magnetism in graphene was detected via AHE measurements (Fig. 5a–f)[63]. The extracted RAHE signal closely matches the magnetic field dependence of the YIG substrate. Subsequent studies reported a maximum R_{AHE} of ≈200 Ω at 2 K and maximal Curie temperature for magnetized graphene close to room temperature.

The induced ferromagnetic order in graphene on YIG was further confirmed by XMCD experiments (Fig. 5g, h)[43]. It is important to note that in both studies, graphene was transferred onto YIG using a polymer stamp, which inevitably introduces contaminants either on the surface or at the graphene/YIG interface. This necessitates careful and systematic characterization of the interfaces using complementary spectroscopic and microscopic techniques[77]. Such contamination is evident in the C *K*-edge NEXAFS spectra of gr/YIG, where additional features related to C = O bonds appear around 286-290 eV, distinct from the expected C $1s \rightarrow \pi^*$ or C $1s \rightarrow \sigma^*$ transitions (see Fig. 5g, h)[78,79]. Following these experimental observations, theoretical analysis of the electronic structure at the graphene/YIG interface was performed[65]. It was found that graphene adsorption on YIG induces *n*-doping and opens a band gap directly at the Dirac point. Due to the interaction with the ferromagnetic substrate

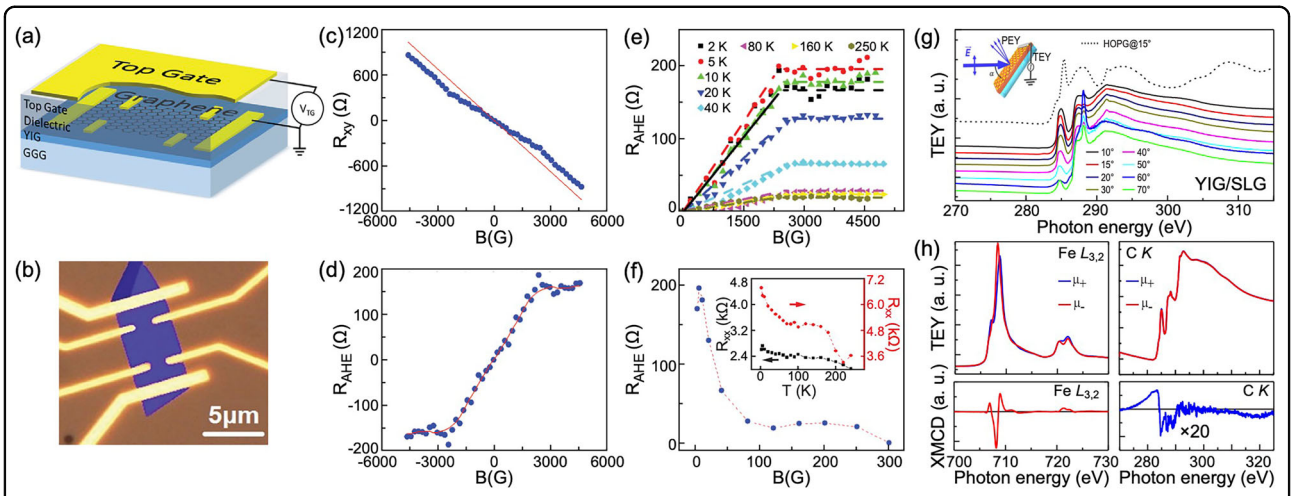

Fig. 5 Properties of the graphene/FMI-YIG interface. a Schematic drawing (with top gate) and **b** optical image (without top gate) of the devices after graphene was transferred to YIG substrate (false color). Magnetic field is perpendicular to the sample plane. **c** The total Hall resistivity data at 2 K (anti-symmetrized) with a straight red line indicating the ordinary Hall background for the gr/YIG system. **d** The nonlinear Hall resistivity after the linear background is removed from the data in (**c**). **e** AHE resistance at different temperatures and **f** the temperature dependence of AHE resistance for gr/YIG. Inset is the longitudinal resistance at the Dirac point with no magnetic field (black) and at 1 T perpendicular magnetic field (red). Data are reproduced from ref. [63]. **g**, **h** C *K* and Fe $L_{2,3}$ NEXAFS and XMCD spectra measured for gr/YIG system. Data are reproduced from ref. [43].

and spin-dependent hybridization between graphene π states and substrate spin-polarized states, spin-dependent band gaps form at the Dirac point: approximately 116 meV for spin-up and 52 meV for spin-down states. Consequently, the spin splitting for electrons and holes in graphene is estimated to be around 52 meV and 115 meV, respectively.

Detailed studies of the gr/TmIG interface reveal behavior similar to that observed in other gr/FMI systems, with induced ferromagnetism detected in the graphene layer (Fig. 6)[66]. Analysis of this interface shows that the spin-splitting energy in magnetized graphene can be strongly influenced by interfacial quality factors such as roughness, defects, dangling bonds, and chemical contaminants. These factors may explain discrepancies between theoretical predictions and experimental results. For example, this effect is evident in the NEXAFS spectra of gr/TmIG presented in Fig. 6c–e, where additional spectral intensity between the C 1$s \rightarrow \pi^*$ and C 1$s \rightarrow \sigma^*$ transitions indicates the presence of contaminants or defects within the graphene layer. Such imperfections can significantly alter the electronic and magnetic properties of the magnetized graphene. Despite these challenges, the experimental data and corresponding analysis clearly demonstrate parallel alignment between the magnetic moments of graphene and the octahedral Fe^{3+} ions in TmIG. This observation is supported by DFT calculations (Fig. 6f), which reveal hybridization between graphene π states and spin-polarized Fe 3*d* states, confirming the induced magnetism in graphene on TmIG. Building on these experimental and theoretical findings, other interfaces of graphene with ferromagnetic pristine and rare-earth doped iron-oxide-based surfaces, like half-metallic ferromagnetic Fe_3O_4[80,81] or Sm- and Ho-substituted nickel ferrites[82], might be of future interest.

To avoid the detrimental effects of contamination and imperfections on the electronic and magnetic properties of gr/FMI systems, direct growth of graphene on an insulator, or vice versa, should be pursued. In this context, ferromagnetic Eu-based chalcogenides (EuX) can be directly grown on graphene. Among these, EuO is often preferred over EuS because of its higher bulk Curie temperature (69 K vs. 16 K). Given the hexagonal lattice of graphene, it is natural to expect that fcc EuO would grow in the (111) orientation on graphene. Therefore, theoretical investigations have focused on EuO(111) and EuS(111) interfaces[65,67]. For EuO/graphene, the exchange splitting of graphene π states is predicted to be approximately 36 meV, with about 24% spin polarization. Substituting EuO with EuS leads to a significant reduction in the exchange splitting, which is attributed to differences in the respective interface structures65. It should be noted that EuO(111) and EuS(111) are polar surfaces that may undergo substantial surface reconstruction, potentially modifying their exchange interaction parameters compared to those predicted by simplified theoretical models.

From an experimental perspective, interfacing EuO with graphene presents significant challenges. Depending on the synthesis conditions, the growth may result in higher oxides such as Eu_3O_4 and Eu_2O_3, or produce a mixture of polar EuO(111) phases along with unintentional Eu intercalation beneath graphene. In ref. [68], textured EuO

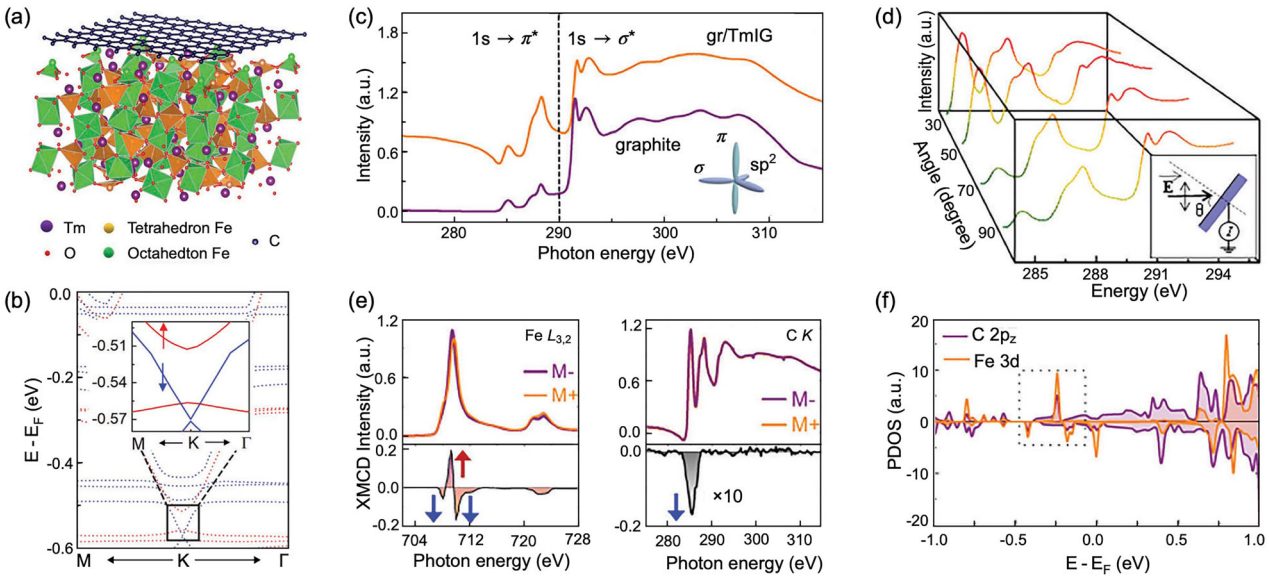

Fig. 6 Properties of the graphene/FMI-TmIG interface. a Supercell for graphene on a $Tm_3Fe_5O_{12}$(111) (TmIG) surface. Blue (the top layer), purple (large), yellow and green (medium), and red (small) colors represent C, Tm, Fe, and O atoms, respectively. **b** Calculated spin-resolved band structure of gr/TmIG heterostructure. Bands in red (blue) correspond to spin up (down). The inset shows the enlargement of the calculated low energy bands at the K point. **c** NEXAFS acquired at the C K-edge of gr/TmIG. **d** Angle-dependent C K-edge NEXAFS spectra of gr/TmIG. **e** XMCD spectra of the gr/TmIG system: Absorption spectra at the Fe $L_{2,3}$- and C *K*-edges are measured at ±2 T magnetic field. The corresponding XMCD signals are shown in the lower panels of the respective figures. **f** The partial density of states (PDOSs) of Fe 3 *d* orbitals and C $2p_z$ orbitals. The dashed square box highlights the overlaps of orbitals. Data are reproduced from ref. [66].

thick films (thickness > 20 nm) were successfully grown on graphene via reactive molecular beam epitaxy. The preferential formation of EuO(001) on graphene was attributed to the minimization of surface energies and the lattice mismatch between EuO and graphene, where EuO's square lattice aligns along the zig-zag directions of the graphene hexagonal lattice (see Fig. 7a). Raman spectroscopy confirmed the structural stability of the graphene lattice after EuO deposition (Fig. 7b). Subsequent electron transport measurements (Fig. 7c, d) revealed a magnetic transition at an elevated temperature $T_C^* \approx 220$ K, accompanied by a strongly non-linear temperature dependence of the transverse resistance R_{xy} up to T_C^*, indicative of an AHE in graphene. Interestingly, this effective Curie temperature T_C^* significantly exceeds the bulk EuO Curie temperature $T_C = 69$ K, contrasting with previous observations in gr/YIG systems[63], where the induced AHE signal suggested a Curie temperature lower than that of YIG. The observation of AHE in the gr/EuO system points to the presence of induced spin-orbit coupling in graphene, arising from hybridization between the electronic states of graphene and EuO. This finding implies that proximity to EuO induces high-temperature magnetism in the graphene layer, as evidenced by transport measurements.

Recent advances in the study of 2D and vdW materials have demonstrated that magnetic order can persist down to the monolayer limit, as observed in materials such as $Cr_2Ge_2Te_6$ (CGT) and $FePS_3$[83–86]. This opens exciting opportunities for integrating graphene with 2D magnetic materials to fabricate heterostructures with tailored magnetic and electronic properties. CGT emerges as a particularly promising candidate for such integration due to its relatively good lattice match with graphene and a moderately high Curie temperature of $T_C = 66$ K[69,70]. DFT calculations have shown that the induced exchange splitting and spin-dependent band gaps in graphene on CGT strongly depend on the relative lattice orientation, with the largest effects on the order of several tenths of meV occurring near a "magic" rotation angle of 19.1°[69]. This behavior is attributed to a particularly strong coupling between spin-down carbon pz orbitals and the lowest spin-down conduction band states of CGT, which are primarily composed of Ge p_z and Cr *d* orbitals. Experimental confirmation of proximity-induced ferromagnetism in the gr/CGT system has been reported through spin-transport measurements[71] and the observation of the AHE in the graphene layer[72].

For interfaces formed between graphene and antiferromagnetic MPX_3 materials, recent DFT calculations predict exchange interactions that can reach up to 10 meV[74,87], making these interfaces promising candidates for observing antiferromagnetic order in the vdW material or induced ferromagnetic order in graphene via

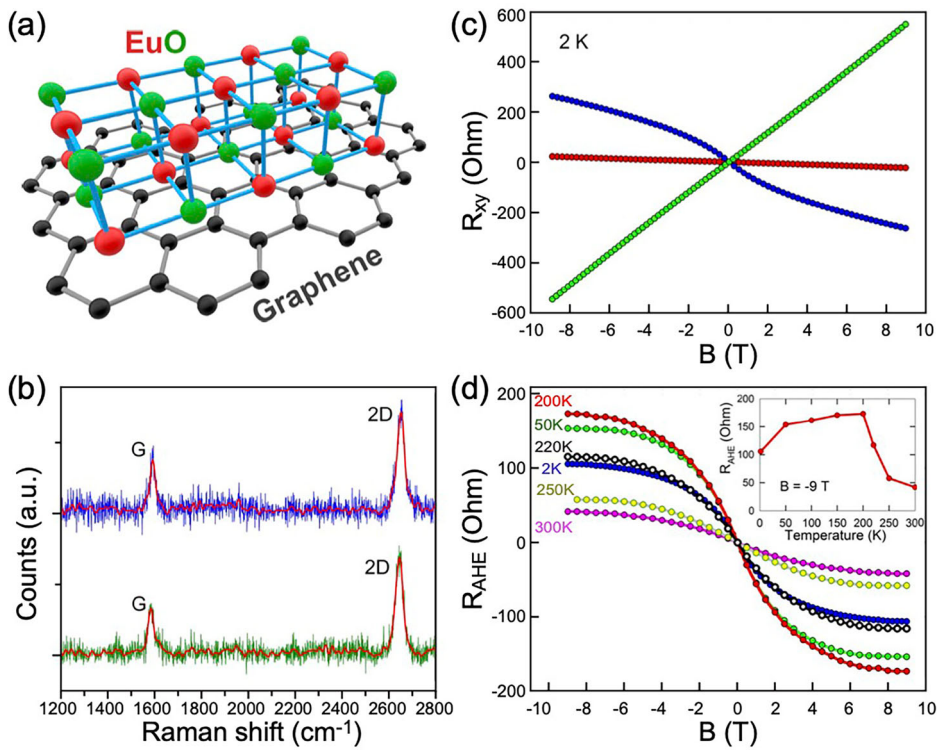

Fig. 7 Properties of the graphene/FMI-EuO interface. a Ball-and-stick model of the structure EuO/graphene showing the relative orientation of the lattices. **b** Raman spectra of graphene before (green) and after (blue) EuO deposition. **c** Magnetic field dependence of transverse resistance in pristine graphene (green), the EuO/graphene structure (blue), and the EuO/graphene (+ Eu) structure (red). **d** Magnetic field dependence of the AHE resistance in the EuO/graphene structure at different temperatures. Inset: temperature dependence of the saturated (taken at −9 T) AHE resistance in the EuO/graphene structure. Data are reproduced from ref. [68].

the AHE. However, existing experimental results remain inconclusive[73,88], highlighting the critical need for careful interface characterization and rigorous analysis of the data obtained[77].

Overall, the interfacial magnetic properties of graphene on different ferromagnetic substrates (FM metal, FMI or FMS) (Fig. 1) are largely governed by two fundamental couplings. The first is the spin-spin exchange interaction between the graphene π electrons and the localized, spin-polarized states of the FM substrate. This mechanism is primarily responsible for the induction of a magnetic moment in carbon atoms and defines whether the graphene spins align parallel or antiparallel to those of the underlying surface. The second is the spin-orbit coupling, which is weak in pristine graphene, but can be strongly enhanced through hybridization with substrates containing heavy elements or transition metals (see e.g., refs. [89] for gr/Au/Co interfaces). At the interface, this induced spin-orbit coupling modifies magnetic anisotropy of the ferromagnetic material, opens spin-dependent gaps in the graphene band structure, and can generate nontrivial spin textures. Taken together, the interplay of spin-spin and spin-orbit interactions dictates the overall character of interface magnetism, offering a pathway to engineer exchange splitting, anisotropy, and even topologically nontrivial states in graphene-based heterostructures.

Conclusions and outlook

The ability to easily tune graphene's electronic structure and induce magnetic order in this purely 2D layer through contact with a FM substrate opens up a wide range of potential applications. These include magnetic sensors based on the theoretically proposed ideal spin-filtering effect in graphene sandwiched between FM layers, as well as optical sensors or switches sensitive to different light polarizations. In this review, we provide an overview of recent progress in the study of various gr/FM-metal and gr/FMI(FMS) interfaces, emphasizing the fundamental mechanisms behind the induced magnetism in graphene. It is now well established that, in both cases, spin-dependent hybridization between graphene's π states and the spin-polarized valence band states of the FM material is responsible for the exchange splitting of graphene's bands and, consequently, the induced magnetic order. Despite significant advances in the synthesis and preparation of gr/FM-metal and gr/FMI(FMS) systems,

several challenges remain. The short- to medium-term prospects for these interfaces in various research and application fields can be summarized as follows:

- In the case of FM/n-ML-gr/FM sandwich structures, an ideal spin-filtering effect has been theoretically predicted due to the alignment of spin-polarized Fermi surfaces. Recent experiments provide encouraging evidence in this direction, such as the observation of spin-filtering in Ni/gr/Ni(111) nanojunctions[11]; however, the "ideal" spin-filtering effect has yet to be conclusively demonstrated. To address the discrepancies between theoretical predictions and experimental realizations, detailed investigations into synthesis methods and thorough characterization of the resulting interfaces are essential. Complementary techniques such as XMCD and spARPES are needed to elucidate the spin texture and magnetic coupling within these junctions.
- Similar questions arise regarding the predicted large exchange splitting of graphene-derived states in graphene layers formed on FM-Mn_5Ge_3. Although the synthesis of such interfaces has recently been demonstrated with relative ease, corresponding spectroscopic studies, such as XMCD and/or spARPES, are still lacking. It is worth noting that the Curie temperature of the underlying FM-Mn_5Ge_3 alloy can be significantly tuned above room temperature through doping with various elements, making the gr/FM-Mn_5Ge_3 interface highly promising for spintronic applications. This system uniquely integrates three components in a single junction: 2D graphene, FM-Mn_5Ge_3, and semiconducting Ge. Furthermore, experimental studies of the spin-filtering effect in FM/gr/FM-Mn_5Ge_3 junctions could provide valuable confirmation of recent theoretical predictions.
- Despite the successes in studying various gr/FM interfaces, the stability of the induced ferromagnetic order in graphene under conditions such as defect formation, elemental doping, or adsorption of different species has not yet been thoroughly investigated. The strength and character of interfacial couplings in graphene are highly sensitive to modifications of the underlying substrate. Defects and impurities can introduce localized magnetic moments or alter the spin polarization of nearby atoms, thereby changing the exchange interaction with graphene π states. Functionalization or adsorption can further modify charge transfer and bonding geometry, which in turn enhances or suppresses spin-spin exchange and spin-orbit coupling. Such tunability highlights the crucial role of interface engineering in controlling the anisotropy, stability, and overall magnitude of proximity-induced magnetism in graphene-based heterostructures. Addressing these factors is crucial, as it will deepen our understanding of these systems and clarify their potential for practical applications in electronics and spintronics devices.
- External perturbations provide an additional degree of control over proximity-induced magnetism in graphene[90,91,92]. Temperature and pressure directly influence hybridization strength at the interface, thereby modifying exchange splitting and magnetic anisotropy. Electric fields and optical excitation can dynamically tune charge transfer and spin polarization, offering routes toward electrically and optically switchable spintronic devices. Moreover, twist angles between graphene and magnetic substrates generate moiré patterns that reshape the interfacial coupling, potentially leading to novel magnetic textures or topological states.
- As briefly mentioned earlier, studying induced magnetism in graphene within gr/FMI or gr/FMS systems requires the fabrication of transport devices. Due to the small size of these junctions, proper characterization can often be overlooked. However, recent studies have demonstrated that the quality of the gr/FMI(FMS) interface and surface plays a critical role in the performance of such junctions and can significantly affect the observed phenomena. Therefore, thorough characterization of the gr/FMI(FMS) interfaces at every stage of preparation is essential, employing a range of spectroscopic and microscopic techniques. It is also important to highlight that, in all cases, real-space-resolved spectromicroscopy methods[93–96] are crucial for understanding the mechanisms governing electron exchange at the gr/FM interface.
- All of the directions outlined above concerning the experimental investigation of graphene/FM-metal and gr/FMI(FMS) interfaces must be complemented by accurate and well-founded theoretical studies. In this context, constructing an appropriate model is crucial. Graphene has a very low density of states around the Fermi energy in the charge-neutral state, and even small variations in the lattice constant of graphene or the substrate, as well as in the interlayer distance, can lead to dramatic modifications in the electronic structure of the heterostructure. For magnetic substrates, a sufficient thickness is generally required to reproduce all relevant characteristics. The equilibrium graphene–substrate distance can now be reliably reproduced by modern computational methods that account for dispersion interactions. Once such a robust theoretical

description is established, computer modeling can effectively predict new interface properties. Moreover, modern computational resources make it possible to simulate a wide range of experimental conditions, including defect formation, adsorption of various species, applied pressure, and external fields. If promising results are identified in silico, they can subsequently be verified through real experiments.

Acknowledgements
E.V. acknowledges the support by the European Union's NextGenerationEU program. Y.D. acknowledges the support by the project Centre for Advanced Laser Techniques (CALT), co-funded by the European Union through the European Regional Development Fund under the Competitiveness and Cohesion Operational Programme (Grant No. KK.01.1.1.05.0001). The authors acknowledge financial support from the European Regional Development Fund for the project "Materials for clean energy, advanced sensors and quantum technologies" (Grant No. PK.1.1.10.0002).

Author contributions
Elena Voloshina: conceptualization (equal); writing—original draft (equal); writing—review and editing (equal). Yuriy Dedkov: conceptualization (equal); writing—original draft (equal); writing—review and editing (equal).

Competing interests
The authors declare no competing interests.

Received: 19 June 2025 Revised: 14 November 2025 Accepted: 3 February 2026
Published online: 02 March 2026

References

1. Novoselov, K. S. et al. Two-dimensional gas of massless Dirac fermions in graphene. *Nature* **438**, 197–200 (2005).
2. Zhang, Y., Tan, Y.-W., Stormer, H. L. & Kim, P. Experimental observation of the quantum Hall effect and Berry's phase in graphene. *Nature* **438**, 201–204 (2005).
3. Geim, A. K. & Novoselov, K. S. The rise of graphene. *Nat. Mater.* **6**, 183–191 (2007).
4. Neto, A. H. C., Guinea, F., Peres, N. M. R., Novoselov, K. S. & Geim, A. K. The electronic properties of graphene. *Rev. Mod. Phys.* **81**, 109–162 (2009).
5. Andrei, E. Y., Li, G. & Du, X. Electronic properties of graphene: a perspective from scanning tunneling microscopy and magnetotransport. *Rep. Prog. Phys.* **75**, 056501 (2012).
6. Naumis, G. G., Barraza-Lopez, S., Oliva-Leyva, M. & Terrones, H. Electronic and optical properties of strained graphene and other strained 2D materials: a review. *Rep. Prog. Phys.* **80**, 096501 (2017).
7. Tombros, N., Jozsa, C., Popinciuc, M., Jonkman, H. T. & van Wees, B. J. Electronic spin transport and spin precession in single graphene layers at room temperature. *Nature* **448**, 571–574 (2007).
8. Bisswanger, T. et al. CVD bilayer graphene spin valves with 26 µm spin diffusion length at room temperature. *Nano Lett.* **22**, 4949–4955 (2022).
9. Karpan, V. M. et al. Graphite and graphene as perfect spin filters. *Phys. Rev. Lett.* **99**, 176602 (2007).
10. Karpan, V. M. et al. Theoretical prediction of perfect spin filtering at interfaces between close-packed surfaces of Ni or Co and graphite or graphene. *Phys. Rev. B* **78**, 195419 (2008).
11. Qiu, W. et al. Spin-tunneling magnetoresistive effects in bottom-up-grown Ni/graphene/Ni nanojunctions. *ACS Appl. Mater. Interfaces* **16**, 62509–62515 (2024).
12. Yazyev, O. V. & Helm, L. Defect-induced magnetism in graphene. *Phys. Rev. B* **75**, 125408 (2007).
13. Nair, R. et al. Dual origin of defect magnetism in graphene and its reversible switching by molecular doping. *Nat. Commun.* **4**, 2010 (2013).
14. Romero-Muniz, C., Pou, P. & Perez, R. Induced magnetism in oxygen-decorated N-doped graphene. *Carbon* **159**, 102–109 (2020).
15. Lin, H., Fratesi, G. & Brivio, G. P. Graphene magnetism induced by covalent adsorption of aromatic radicals. *Phys. Chem. Chem. Phys.* **17**, 2210–2215 (2014).
16. Gonzalez-Herrero, H. et al. Atomic-scale control of graphene magnetism by using hydrogen atoms. *Science* **352**, 437–441 (2016).
17. Sun, Y. et al. Magnetism of graphene quantum dots. *npj Quantum Mater.* **2**, 5 (2017).
18. Hu, W. et al. Room-temperature magnetism and tunable energy gaps in edge-passivated zigzag graphene quantum dots. *npj 2D Mater. Appl.* **3**, 17 (2019).
19. Yazyev, O. V. Emergence of magnetism in graphene materials and nanostructures. *Rep. Prog. Phys.* **73**, 056501 (2010).
20. Manna, P. & Yusuf, S. Two interface effects: exchange bias and magnetic proximity. *Phys. Rep.* **535**, 61–99 (2014).
21. Yang, K., Huang, W.-Q., Hu, W., Huang, G.-F. & Wen, S. Substrate-induced magnetism and topological phase transition in silicene. *Nanoscale* **10**, 14667–14677 (2018).
22. Field, B., Schiffrin, A. & Medhekar, N. V. Correlation-induced magnetism in substrate-supported 2D metal-organic frameworks. *npj Comput. Mater.* **8**, 227 (2022).
23. Li, Z., Li, S., Xu, Y. & Tang, N. Recent advances in magnetism of graphene from 0D to 2D. *Chem. Commun.* **59**, 6286–6300 (2023).
24. Bertoni, G., Calmels, L., Altibelli, A. & Serin, V. First-principles calculation of the electronic structure and EELS spectra at the graphene/Ni(111) interface. *Phys. Rev. B* **71**, 075402 (2005).
25. Gamo, Y., Nagashima, A., Wakabayashi, M., Terai, M. & Oshima, C. Atomic structure of monolayer graphite formed on Ni(111). *Surf. Sci.* **374**, 61–64 (1997).
26. Parreiras, D. E. et al. Graphene/Ni(111) surface structure probed by low-energy electron diffraction, photoelectron diffraction, and first-principles calculations. *Phys. Rev. B* **90**, 155454 (2014).
27. Voloshina, E. N. et al. Structural and electronic properties of the graphene/Al/Ni(111) intercalation system. *N. J. Phys.* **13**, 113028 (2011).
28. Voloshina, E. & Dedkov, Y. in *Physics and Applications of Graphene* (ed. Mikhailov, S.) 329–352 (InTech, 2011).
29. Voloshina, E. et al. Electronic structure and magnetic properties of graphene/Ni_3Mn/Ni(111) trilayer. *J. Phys. Chem. C.* **123**, 4994–5002 (2019).
30. Yue, W., Guo, Q., Dedkov, Y. & Voloshina, E. Electronic and magnetic properties of the graphene/Y/Co(0001) interfaces: insights from the density functional theory analysis. *ACS Omega* **7**, 7304–7310 (2022).
31. Voloshina, E. N. & Dedkov, Y. S. General approach to understanding the electronic structure of graphene on metals. *Mater. Res. Express* **1**, 035603 (2014).
32. Usachov, D. et al. Observation of single-spin Dirac fermions at the graphene/ferromagnet interface. *Nano Lett.* **15**, 2396–2401 (2015).
33. Marchenko, D. et al. Highly spin-polarized Dirac fermions at the graphene/Co interface. *Phys. Rev. B* **91**, 235431 (2015).
34. Batzill, M. The surface science of graphene: metal interfaces, CVD synthesis, nanoribbons, chemical modifications, and defects. *Surf. Sci. Rep.* **67**, 83–115 (2012).
35. Dedkov, Y. & Voloshina, E. Graphene growth and properties on metal substrates. *J. Phys. Condens. Matter* **27**, 303002 (2015).
36. Yang, M., Liu, Y., Fan, T. & Zhang, D. Metal-graphene interfaces in epitaxial and bulk systems: a review. *Prog. Mater. Sci.* **110**, 100652 (2020).
37. Weser, M. et al. Induced magnetism of carbon atoms at the graphene/Ni(111) interface. *Appl. Phys. Lett.* **96**, 012504 (2010).
38. Dedkov, Y. S. & Fonin, M. Electronic and magnetic properties of the graphene–ferromagnet interface. *N. J. Phys.* **12**, 125004 (2010).
39. Weser, M., Voloshina, E. N., Horn, K. & Dedkov, Y. S. Electronic structure and magnetic properties of the graphene/Fe/Ni(111) intercalation-like system. *Phys. Chem. Chem. Phys.* **13**, 7534–7539 (2011).
40. Matsumoto, Y. et al. Spin orientation transition across the single-layer graphene/nickel thin film interface. *J. Mater. Chem. C.* **1**, 5533–5537 (2013).
41. Vita, H. et al. Electronic structure and magnetic properties of cobalt intercalated in graphene on Ir(111). *Phys. Rev. B* **90**, 165432 (2014).
42. Mertins, H.-C. et al. Giant magneto-optical Faraday effect of graphene on Co in the soft X-ray range. *Phys. Rev. B* **98**, 064408 (2018).
43. Mendes, J. B. S. et al. Direct detection of induced magnetic moment and efficient spin-to-charge conversion in graphene/ferromagnetic structures. *Phys. Rev. B* **99**, 214446 (2019).

44. Aboljadayel, R. O. M. et al. Determining the proximity effect induced magnetic moment in graphene by polarized neutron reflectivity and x-ray magnetic circular dichroism. *ACS Appl. Mater. Interfaces* **15**, 22367–22376 (2023).
45. Aboljadayel, R. O. M. et al. Measurement of the induced magnetic polarisation of rotated-domain graphene grown on Co film with polarised neutron reflectivity. *Nanomaterials* **13**, 2620 (2023).
46. Srivastava, P. et al. Magnetic moments and Curie temperatures of Ni and Co thin films and coupled trilayers. *Phys. Rev. B* **58**, 5701–5706 (1998).
47. Gao, M. et al. Graphene-mediated ferromagnetic coupling in the nickel nano-islands/graphene hybrid. *Sci. Adv.* **7**, eabg7054 (2021).
48. Xiao, R. et al. Co dimers on hexagonal carbon rings proposed as sub-nanometer magnetic storage bits. *Phys. Rev. Lett.* **103**, 187201 (2009).
49. Rougemaille, N. et al. Perpendicular magnetic anisotropy of cobalt films intercalated under graphene. *Appl. Phys. Lett.* **101**, 142403 (2012).
50. Yang, H. et al. Anatomy and giant enhancement of the perpendicular magnetic anisotropy of cobalt–graphene heterostructures. *Nano Lett.* **16**, 145–151 (2016).
51. Dedkov, Y. S. et al. Intercalation of copper underneath a monolayer of graphite on Ni(111). *Phys. Rev. B* **64**, 035405 (2001).
52. Gruneis, A. & Vyalikh, D. V. Tunable hybridization between electronic states of graphene and a metal surface. *Phys. Rev. B* **77**, 193401 (2008).
53. Varykhalov, A., Scholz, M. R., Kim, T. K. & Rader, O. Effect of noble-metal contacts on doping and band gap of graphene. *Phys. Rev. B* **82**, 121101 (2010).
54. Vilkov, O. et al. Controlled assembly of graphene-capped nickel, cobalt and iron silicides. *Sci. Rep.* **3**, 2168 (2013).
55. Dedkov, Y. et al. Decoupling of graphene from Ni(111) via formation of an interfacial NiO layer. *Carbon* **121**, 10–16 (2017).
56. Pozzo, M. et al. Interplay among hydrogen chemisorption, intercalation, and bulk diffusion at the graphene-covered Ni(111) crystal. *J. Phys. Chem. C.* **127**, 6938–6947 (2023).
57. Voloshina, E. N. & Dedkov, Y. S. Electronic and magnetic properties of the graphene/Eu/Ni(111) hybrid system. *Z. Naturforsch. A* **69**, 297–302 (2014).
58. Voloshina, E. & Dedkov, Y. Dirac electron behavior for spin-up electrons in strongly interacting graphene on ferromagnetic Mn_5Ge_3. *J. Phys. Chem. Lett.* **10**, 3212–3216 (2019).
59. Zhang, J., Paulus, B., Dedkov, Y. & Voloshina, E. Proximity effects in the graphene-$Co_3Sn_2S_2$ interface. *J. Mater. Chem. C.* **13**, 11789–11799 (2025).
60. Jugovac, M. et al. Inducing single spin-polarized flat bands in monolayer graphene. *Adv. Mater.* **35**, e2301441 (2023).
61. Sheverdyaeva, P. M. et al. Spin-dependent $\pi\pi^*$ gap in graphene on a magnetic substrate. *Phys. Rev. Lett.* **132**, 266401 (2024).
62. Dedkov, Y. et al. Realization of a new graphene-ferromagnet interface with Dirac linear band dispersion. *ACS Appl. Mater. Interfaces* **15**, 26190–26198 (2023).
63. Wang, Z., Tang, C., Sachs, R., Barlas, Y. & Shi, J. Proximity-induced ferromagnetism in graphene revealed by the anomalous Hall effect. *Phys. Rev. Lett.* **114**, 016603 (2015).
64. Leutenantsmeyer, J. C., Kaverzin, A. A., Wojtaszek, M. & Van. Wees, B. J. Proximity induced room temperature ferromagnetism in graphene probed with spin currents. *2D Mater.* **4**, 014001 (2016).
65. Hallal, A., Ibrahim, F., Yang, H., Roche, S. & Chshiev, M. Tailoring magnetic insulator proximity effects in graphene: first-principles calculations. *2D Mater.* **4**, 025074 (2017).
66. Hu, J. et al. Tunable spin-polarized states in graphene on a ferrimagnetic oxide insulator. *Adv. Mater.* **36**, e2305763 (2024).
67. Yang, H. X. et al. Proximity effects induced in graphene by magnetic insulators: first-principles calculations on spin filtering and exchange-splitting gaps. *Phys. Rev. Lett.* **110**, 046603 (2013).
68. Averyanov, D. V. et al. High-temperature magnetism in graphene induced by proximity to EuO. *ACS Appl. Mater. Interfaces* **10**, 20767–20774 (2018).
69. Zollner, K. & Fabian, J. Engineering proximity exchange by twisting: reversal of ferromagnetic and emergence of antiferromagnetic Dirac bands in graphene/$Cr_2Ge_2Te_6$. *Phys. Rev. Lett.* **128**, 106401 (2022).
70. Zollner, K., Gmitra, M. & Fabian, J. Electrically tunable exchange splitting in bilayer graphene on monolayer $Cr_2X_2Te_6$ with X = Ge, Si, and Sn. *N. J. Phys.* **20**, 073007 (2018).
71. Karpiak, B. et al. Magnetic proximity in a van der Waals heterostructure of magnetic insulator and graphene. *2D Mater.* **7**, 015026 (2020).
72. Yao, S. et al. Observation of the anomalous Hall effect in proximity coupled $Cr_2Ge_2Te_6$/graphene heterostructures. *Nanoscale* **17**, 5878–5887 (2025).
73. Zhang, Y. et al. $MnPS_3$ spin-flop transition-induced anomalous Hall effect in graphite flake via van der Waals proximity coupling. *Nanoscale* **12**, 23266–23273 (2020).
74. Zollner, K. & Fabian, J. Proximity effects in graphene on monolayers of transition-metal phosphorus trichalcogenides MPX_3 (M: Mn, Fe, Ni, Co, and X: S, Se). *Phys. Rev. B* **106**, 035137 (2022).
75. Nagaosa, N., Sinova, J., Onoda, S., MacDonald, A. H. & Ong, N. P. Anomalous Hall effect. *Rev. Mod. Phys.* **82**, 1539–1592 (2010).
76. Bora, M. & Deb, P. Magnetic proximity effect in two-dimensional van der Waals heterostructure. *J. Phys. Mater.* **4**, 034014 (2021).
77. Dedkov, Y. & Voloshina, E. On the study of proximity magnetism in van der Waals graphene/$CuCrP_2S_6$ heterostructure via the anomalous Hall effect. *Appl. Phys. Rev.* **11**, 041409 (2024).
78. Gandhiraman, R. P. et al. X-ray absorption study of graphene oxide and transition metal oxide nanocomposites. *J. Phys. Chem. C.* **118**, 18706–18712 (2014).
79. Ehlert, C., Unger, W. E. S. & Saalfrank, P. C K-edge NEXAFS spectra of graphene with physical and chemical defects: a study based on density functional theory. *Phys. Chem. Chem. Phys.* **16**, 14083–14095 (2014).
80. Dedkov, Y. S., Rüdiger, U. & Güntherodt, G. Evidence for the half-metallic ferromagnetic state of Fe_3O_4 by spin-resolved photoelectron spectroscopy. *Phys. Rev. B* **65**, 064417 (2002).
81. Liao, Z.-M. et al. Magnetoresistance of Fe_3O_4-graphene-Fe_3O_4 junctions. *Appl. Phys. Lett.* **98**, 052511 (2011).
82. Bharathi, K. K., Markandeyulu, G. & Ramana, C. V. Structural, magnetic, electrical, and magnetoelectric properties of Sm- and Ho-substituted nickel ferrites. *J. Phys. Chem. C.* **115**, 554–560 (2011).
83. Gong, C. et al. Discovery of intrinsic ferromagnetism in two-dimensional van der Waals crystals. *Nature* **546**, 265–269 (2017).
84. Wang, X. et al. Raman spectroscopy of atomically thin two-dimensional magnetic iron phosphorus trisulfide ($FePS_3$) crystals. *2D Mater.* **3**, 031009 (2016).
85. Jiang, X. et al. Recent progress on 2D magnets: fundamental mechanism, structural design and modification. *Appl. Phys. Rev.* **8**, 031305 (2021).
86. Dedkov, Y., Guo, Y. & Voloshina, E. Progress in the studies of electronic and magnetic properties of layered MPX_3 materials (M: transition metal, X: chalcogen). *Electron. Struct.* **5**, 043001 (2023).
87. Hogl, P. et al. Quantum anomalous Hall effects in graphene from proximity-induced uniform and staggered spin-orbit and exchange coupling. *Phys. Rev. Lett.* **124**, 136403 (2020).
88. Tang, W. et al. Unveiling magnetism in individual $CuCrP_2S_6$ flakes by magnetic proximity effect. *Appl. Phys. Rev.* **10**, 031404 (2023).
89. Rybkin, A. G. et al. Sublattice ferrimagnetism in quasi freestanding graphene. *Phys. Rev. Lett.* **129**, 226401 (2022).
90. Popov, I., Mantega, M., Narayan, A. & Sanvito, S. Proximity-induced topological state in graphene. *Phys. Rev. B* **90**, 035418 (2014).
91. Naimer, T., Zollner, K., Gmitra, M. & Fabian, J. Twist-angle dependent proximity induced spin-orbit coupling in graphene/transition metal dichalcogenide heterostructures. *Phys. Rev. B* **104**, 195156 (2021).
92. Fulop, B. et al. Boosting proximity spin-orbit coupling in graphene/WSe_2 heterostructures via hydrostatic pressure. *npj 2D Mater. Appl.* **5**, 82 (2021).
93. Jones, A. J. H. et al. Observation of electrically tunable van Hove singularities in twisted bilayer graphene from nanoARPES. *Adv. Mater.* **32**, e2001656 (2020).
94. Hofmann, P. Accessing the spectral function of in operando devices by angle-resolved photoemission spectroscopy. *AVS Quantum Sci.* **3**, 021101 (2021).
95. Jiang, Z. et al. Revealing flat bands and hybridization gaps in a twisted bilayer graphene device with microARPES. *2D Mater.* **10**, 045027 (2023).
96. Guo, Y. et al. Electronic properties of graphene interfaced with multiferroic van der Waals $CuCrP_2S_6$ from X-ray spectromicroscopy and DFT. *Carbon* **234**, 119974 (2025).